Electromagnetic fluctuations during guide field reconnection in a laboratory plasma

A. v. Stechow,[1] W. Fox,[2] J. Jara-Almonte,[2] J. Yoo,[2] H. Ji,[2] and M. Yamada[2]
[1]*Max Planck Institute for Plasma Physics, Wendelsteinstraße 1, 17491 Greifswald, Germany*
[2]*Princeton Plasma Physics Laboratory, Princeton, New Jersey 08543, USA*

(Received 13 February 2018; accepted 25 April 2018; published online 23 May 2018)

Electromagnetic fluctuations are studied during magnetic reconnection in a laboratory plasma for a range of guide magnetic fields from nearly zero up to normalized guide fields $B_g/B_{up} = 1.2$. The predominant fluctuations are identified as right-hand polarized whistler modes, which become increasingly organized and less intermittent, and obtain larger amplitude with the increasing guide field. The fluctuation amplitude also increases with the reconnecting magnetic field, implying a relatively constant conversion of upstream magnetic energy to turbulent fluctuations of $\lesssim 1\%$ across guide field strengths. *Published by AIP Publishing*. https://doi.org/10.1063/1.5025827

I. INTRODUCTION

Magnetic reconnection plays an important role in magnetized plasmas from the laboratory to astrophysics.[1] It allows a change in magnetic topology which in turn can lead to explosive release of stored magnetic energy, including solar flares[2] and magnetospheric plasmas.[3] In magnetic confinement experiments, reconnection controls the self-organization of plasmas, for example, the change in topology from reconnection allows the fast heat transport associated with the sawtooth crash.[4–6] During reconnection, a narrow (on global scales) current sheet forms between regions of opposing magnetic field; in the current sheet, the frozen-in flux condition is violated, allowing magnetic field lines to break and change topology. Reconnection can allow the efficient transfer of magnetic energy to the plasma by heating it, driving plasma flows, and can energize fast particle populations in collisionless regimes through large electric fields associated with the magnetic reorganization.

In many systems, magnetic reconnection proceeds in the presence of a guide magnetic field, such that the merging fields meet at an angle less than 180°, i.e., they are not completely anti-parallel. Guide field (GF) reconnection is typical of solar flares; at the magnetopause, depending on the "clock angle" of the incoming solar wind; and in magnetic fusion devices due to the strong applied toroidal field (TF) which dominates the magnetic fields of the system. Conceptually, the guide field is important because it changes the physics of how plasma and field decouple in the current sheet by providing stronger magnetization of electrons and ions in the current sheet.[7] To understand this physics, a number of dedicated laboratory experiments have studied magnetic reconnection in guide field regimes.[8–14]

In nearly all plasmas of laboratory or observational interest, collisional effects are too weak to account for the electric fields associated with reconnection, and significant effort has attempted to find mechanisms to account for these large electric fields. Furthermore, in reconnection with a guide field, the electric field associated with reconnection obtains a significant parallel component which can efficiently accelerate particles, and it is important to understand how this component is balanced in weakly collisional plasmas. A significant theoretical advance was made nearly 20 years ago by the identification of electron pressure variations with quadrupolar symmetry in two-fluid or extended-MHD simulations which naturally form in reconnection layers thinner than the ion-skin depth.[15–18] The in-plane pressure variations generate a pressure gradient along the total magnetic field which balance the parallel electric field. Recent experiments on the Magnetic Reconnection Experiment (MRX)[13] have now directly measured these pressure structures in magnetic reconnection layers and observed that they indeed balance the measured electric fields.

However, while this mechanism can account for the parallel electric fields over the larger-scale ion-diffusion region, closer to the reconnection X-line and within the electron diffusion region (EDR), these two-fluid mechanisms themselves break down, requiring yet an additional mechanism to balance parallel electric fields there. The recent MRX experiments indeed identified the EDR as extending to approximately 1 ρ_s in the outflow direction in which the parallel electric field was significantly imbalanced. The proposed mechanisms to balance the reconnection electric field in the EDR include pressure anisotropy and agyrotropy[19,20] or anomalous dissipation from fluctuations.

These considerations have motivated the experimental study of fluctuations as a mechanism to provide anomalous dissipation, both in laboratory[8,10,14,21–23] and space plasmas (e.g., Refs. 24–26). Recent space experiments, while providing important ground truth for the presence of fluctuations in magnetosphere reconnection, have been limited because the single-pass nature of spacecraft data is not well suited to obtain the statistics necessary to conclusively show the importance of fluctuations for fast reconnection. Therefore, this topic is one where laboratory experiments can provide extremely valuable data on reconnection that is very difficult to obtain by other means.

At MRX, electrostatic and electromagnetic waves were identified in the anti-parallel (zero guide field) reconnection

setup in the lower-hybrid frequency regime.[21,22] These were later identified as whistler-like, obliquely propagating lower hybrid drift instability (LHDI) modes.[27] The LHDI is driven by cross-field, diamagnetic currents which naturally arise during anti-parallel reconnection since the magnetic field is purely perpendicular to the current sheet. These fluctuations were observed to scale with the collisionality and correlated with the resistivity anomaly and were therefore proposed to account for the required anomalous resistivity. In reconnection experiments in guide field regimes, electrostatic fluctuations from the lower-hybrid regime through to the electron cyclotron regime were observed on the Versatile Toroidal Facility (VTF) experiment.[10,23,28] Non-linear electron hole structures were observed,[10] attributed to strong beam-plasma instabilities driven by accelerated electrons[23] in the reconnection layer. Experiments on the strong guide field VINETA.II experiment[14] observed broadband fluctuations in the lower hybrid frequency range propagating with the whistler wave dispersion in the guide field direction. While these were shown to peak at the current sheet center, their wave amplitudes were by far too small to significantly contribute to the reconnection electric field.

In the present work, we study the role of magnetic fluctuations in a series of experiments at the Magnetic Reconnection Experiment which scan the applied guide field in a controlled fashion. Besides the general importance of understanding fluctuations in guide field reconnection regimes, the controllable guide field furthermore provides a new experimental knob to systematically test the role of fluctuations in reconnection. For example, the addition of the guide field also changes the driving mechanisms for the instabilities, since at near zero guide field, the plasma current is nearly entirely cross-field and therefore related to density and temperature gradients, which are well-studied to drive lower-hybrid instabilities. With the addition of the guide field, the current becomes increasingly parallel to the magnetic field. This work complements and extends previous work at MRX which has identified electrostatic[21] and electromagnetic[22] waves during anti-parallel (zero guide field) reconnection.

Reconnection is studied in a low-collisionality regime, where the reconnection electric field E is significantly larger than provided by dissipation due to Spitzer resistivity $\eta_{sp}j$, so that some sort of collisionless or anomalous dissipation is required in the electron diffusion layer. At all guide field values in the present experiments, broadband fluctuations are observed which span the lower hybrid frequency range $[f_{ci} \lesssim f \sim f_{LH} = (f_{ce}f_{ci})^{1/2}]$ with a power law spectrum vs. frequency. Hodogram analysis at the current sheet center shows that at high guide fields, these fluctuations are right-hand polarized, whistler-like waves that propagate at a small angle to the mean field. A striking result is that the fluctuation amplitudes rise sharply as the guide field is increased, with the components increasingly organized perpendicular to the guide field. Spatial scans show that fluctuations peak at the current sheet center, correlating well with the current density profiles, which is a positive indicator that they could be associated with anomalous dissipation. However, the amplitude of the waves varies strongly with the guide field, despite physical reconnection rates which are relatively constant; this does not mesh well with the idea that the waves provide significant anomalous resistivity across all guide fields or indicate deficiencies in the simplest models for estimating anomalous resistivity from wave amplitudes. This will be elaborated and put in context of other reconnection experiments in Sec. IV.

The remainder of this paper is organized as follows: Section II reviews the MRX experiment in its guide field setup and introduces the data analysis methods to process and characterize intermittent fluctuations from large datasets. Section III characterizes the magnetic fluctuations in relation to the guide field. First, the overall reconnection parameter variations with changes to the guide field are characterized. Next, spatial profiles and spectra of fluctuations are presented as a function of guide field. Finally, a detailed analysis of the wave polarization and propagation direction at the current sheet center is presented. Section IV then discusses these results in relation to previous findings and as a possible mechanism to provide anomalous resistivity.

II. EXPERIMENTAL SETUP AND METHODS

A. Device overview

MRX is a toroidal laboratory reconnection experiment[29] that has been upgraded to study guide field reconnection. Figure 1 shows a schematic cross-section of the toroidally symmetric device. For the toroidal coordinate, Y and Θ are used interchangeably, while the axial and radial coordinates are labeled Z and R, respectively. The flux cores possess separate poloidal field (PF) and toroidal field (TF) windings. During an experimental shot, the PF coils first generate a poloidal field in the vacuum chamber, corresponding to the flux contours shown in the diagram. The plasma is subsequently generated by induction by pulsing the TF coils. Next, to drive reconnection, the PF coil current is ramped down over the course of several tens of μs, which pulls magnetic flux towards the flux cores, creating a central current sheet as indicated in the figure. Equilibrium field (EF) coils mounted external to the vacuum chamber provide a counter to the hoop force to control the radial position of the current sheet. Previous investigations of energy conversion during

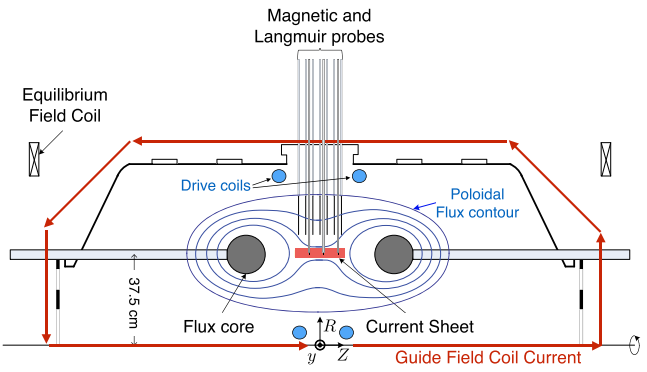

FIG. 1. Schematic cross-section of MRX including the contour of the vacuum chamber, the various internal and external coils, the probe locations as well as sample poloidal flux countours together with the reconnecting current sheet.

zero guide field reconnection[29] show that around half of the magnetic energy inflow rate (2 MW) is converted to particle energy, of which 2/3 is deposited into the ions and the remainder into the electrons.

Recent experiments use an additional set of guide field (GF) coils which run through the central column of the experiment and create an additional toroidal field that rolls off in vacuum with a $1/R$ profile.[12,13] During the experiment, plasma motion compresses the guide field in the current sheet and in the reconnection downstream resulting in an increase in the GF compared to the vacuum value. (Hereafter, references to the guide field value correspond to the total, measured guide field rather than that initially applied, except when noted.) Typical values of the compressed GF during reconnection range from 0 to 40 mT, which corresponds to a normalized guide field, $B_g/B_{up} \approx 2$, where B_{up} is the upstream, reconnecting field. The maximum guide field is limited by mechanical constraints as the conductors experience increasing $j \times B$ forces. Finally, in addition to the GF coils, an additional set of poloidal field driving coils have been installed, which provide an additional source of poloidal flux and reconnection drive from the upstream,[13,30] complementing the reconnection drive from the PF coils. This increases the achievable driving inductive field E_Θ and was found to help stabilize the Z-position of the X-point, reducing an effect that had previously complicated the interpretation of guide field reconnection shots.

A set of standard diagnostics installed at MRX provide measurements of magnetic fields as well as plasma density and electron temperature data. These include a stationary 2D array of three-component magnetic pickup loops in the (R, Z)-plane from which the poloidal magnetic flux function and local current density are reconstructed and a set of 3 radially scannable Langmuir probes. In these experiments, these are used to measure the plasma parameters upstream, downstream, and within the reconnecting current sheet. Magnetic fluctuations are measured with additional tri-axis, high frequency magnetic probes[22] which have battery-powered buffer amplifiers in the probe shaft near the probes to minimize transmission line effects. These can be radially scanned between shots to measure profiles of fluctuations and have a coil separation of a few mm which enables reconstruction of local hodograms of the magnetic field vector.[8]

B. Fluctuation data processing

While many overall plasma parameters are reproducible on a shot-to-shot basis, the magnetic fluctuations are found to be highly intermittent. Furthermore, they are not always observed at the same time point during a shot, due to the varying trajectory of the current sheet relative to the stationary magnetic probe. A large number of shots are therefore required for a statistically significant interpretation of results, which generates a large amount of raw data due to high sampling rates.

The raw signals are pre-processed by a wavelet transform in order to simplify subsequent analysis. A complex-valued Morlet wavelet is used[31] that has the advantage of being conceptually similar to a Fourier transform in that the wavelet coefficients $S(\omega, t)$ with frequency scale ω can easily be related to a spectral power value $\hat{B}^2(\omega, t)$ by applying the correct normalization and probe transfer function. The 2D wavelet coefficients are precalculated and stored for fast retrieval in a given $(\Delta t, \Delta\omega)$ window during further analysis. The probe's transfer function $S(\omega) = U(\omega)/B(\omega)$ (where U is the probe voltage) is known from calibration measurements in a Helmholtz field at different frequencies and was found to be linear up to 10 MHz, i.e., $S = i\omega NA$, where N is the number of windings and A is the probe area. Absolute fluctuation amplitudes in a given time window and frequency range are therefore calculated by extracting the corresponding wavelet coefficients, averaging over time, dividing by the transfer function to receive the time-averaged spectra and finally summing over the frequency components.

While single time hodograms can be found in which the waves are coherent for at least one cycle, this is not the norm. To automate the search for these features, we apply a statistical wavelet-based hodogram processing method which identifies the dominant direction (but not magnitude) of the wave vector $\hat{\mathbf{k}}$ and wave polarization from the components of $\tilde{\mathbf{B}}$. This novel processing method[30] uses the fact that $\nabla \cdot \mathbf{B} = 0$, $\mathbf{k} \propto \mathbf{B}(t) \times \mathbf{B}(t + dt)$, within the plane-wave approximation. Conceptually, the magnetic field vector is transverse to the propagation vector and rotates around it. The individual probe signals are wavelet transformed, yielding wavelet coefficients $\hat{B}_i(t, \omega)$ for each time point and frequency. A coordinate system can be found which is aligned with the instantaneous $\mathbf{k}(t, \omega)$ by rotating around two angles θ and ϕ: $(\hat{B}_x, \hat{B}_y, \hat{B}_z) = R(\theta, \phi) \cdot (b_1, b_2)$ with

$$R = \begin{bmatrix} \cos\phi & -\cos\theta\sin\phi \\ \sin\phi & \cos\theta\sin\phi \\ 0 & \sin\theta \end{bmatrix}$$

and unknown complex numbers b_1 and b_2. This finally yields a normalized wave vector $\mathbf{k} = (\sin\theta\sin\phi, -\sin\theta\cos\phi, \cos\theta)$, and the solutions for b_1 and b_2 can be used to define a signed polarization $\varepsilon(\omega, t)$ with respect to the equlibrium field B_0 that ranges from -1 (L-polarized) to 1 (R-polarized), where 0 is a linearly polarized wave. The results over many time windows and shots are accumulated in 2D histograms in (ω, Θ) or (ω, ε) space with $\Theta = \angle(k, B_0)$, revealing spectrally resolved statistics on propagation directions and polarizations.

Since the reconstruction of spatial profiles requires a high degree of reproducibility of the plasma parameters, especially of the current sheet trajectory, either a very large amount of shots or a more sophisticated averaging method is required. Here, we use a Monte-Carlo based averaging method as used in Ref. 13. This allows for a more broad preselection of shots by relaxing the requirement of a strictly centered X-point position for each shot. Instead, only the steady-state phase is identified for each shot, and the spatial coordinates (R, Z) are transformed to a system relative to the measured X-point. The shot-to-shot variations in current sheet localization therefore result in scattered positions of the fixed probes. These separate datasets are then combined for averaging on a single spatial grid by applying a Gaussian

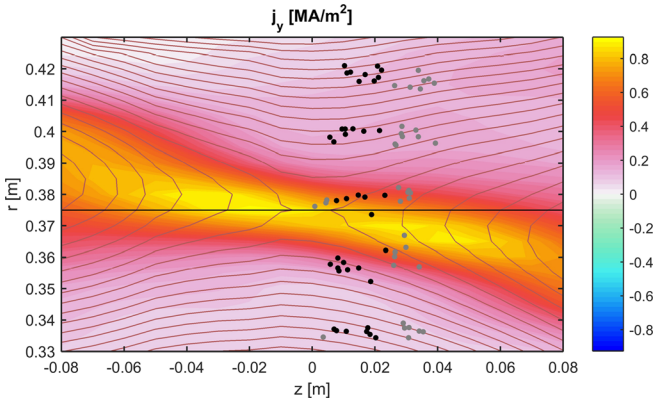

FIG. 2. Averaged current density profile in the poloidal plane (colors) with flux contours (lines) and corrected fluctuation probe locations (dots), at normalized guide field $B_g/B_{up} = 1.3$.

spatial weighting function $S(r) = \exp\left[-(\mathbf{r} - \mathbf{r}_0)^2/\sigma^2\right]$ with $\sigma = 1.5$ cm to each data point $A(\mathbf{r})$ and summing over these values at each grid point

$$A(R,Z) = \frac{\sum_i A(r_i)S(r_i)}{\sum_i S(r_i)}. \quad (1)$$

A statistical error is then obtained by selecting random subsets of the entire dataset and repeating the analysis for each of these realizations. Error bars and confidence intervals can then be constructed from this set of analyzed data to provide an estimate of the error bars associated with both the measurement and this method of reconstruction.

Figure 2 shows an example of this data analysis method which is furthermore relevant to the magnetic fluctuation spatial profiles obtained below. Here, 50 shots at a single guide field setting ($B_g = 30$ mT, $B_g/B_{up} = 1.3$) were combined, in which the radial fluctuation probe was scanned over 5 positions. For each shot, the coordinate system has been adjusted to center the X-point at $(R = 0.375, Z = 0)$, resulting in the corrected probe positions marked by dots. The gray dots denote points that are excluded from the subsequent fluctuation profile reconstruction due to large horizontal X-point shift in these shots. The averaged, X-point corrected current density profile (color) together with the poloidal magnetic flux contours (lines) shows the typical characteristics of guide field reconnection in the two-fluid MHD regime: a long, thin ($\delta \approx 20$ mm full thickness) current sheet which is profoundly tilted with respect to the flux surfaces. This tilt results from $j \times B_g$ forces between the Hall current and the guide field[12] and is also related to the development of the characteristic quadrupolar pressure perturbation.[13]

In comparison, the radial density profile is known from previous investigations[13] to be broad, and Langmuir probe measurements in the upstream region show that the current sheet is indeed embedded within a plasma in which ideal MHD holds, with a density comparable to that at the X-line. Additionally, the previously mentioned quadrupolar structure significantly alters the 2D density profile away from the X-line as the guide field is increased.

III. CHARACTERIZATION OF MAGNETIC FLUCTUATIONS

We now present results of experiments characterizing magnetic fluctuations and their dependence on the guide magnetic field in MRX. First, we document the overall plasma and reconnection parameter variation with changes to the guide field. Next, spatial profiles and power spectra of the fluctuations are presented at three characteristic guide field values. Finally, we report an additional extended dataset where hodogram results are used to identify wave polarization and propagation directions.

Figure 3 shows time traces of a typical MRX shot in which magnetic fluctuations occur. Characteristic plasma parameters in the reconnection layer are densities of

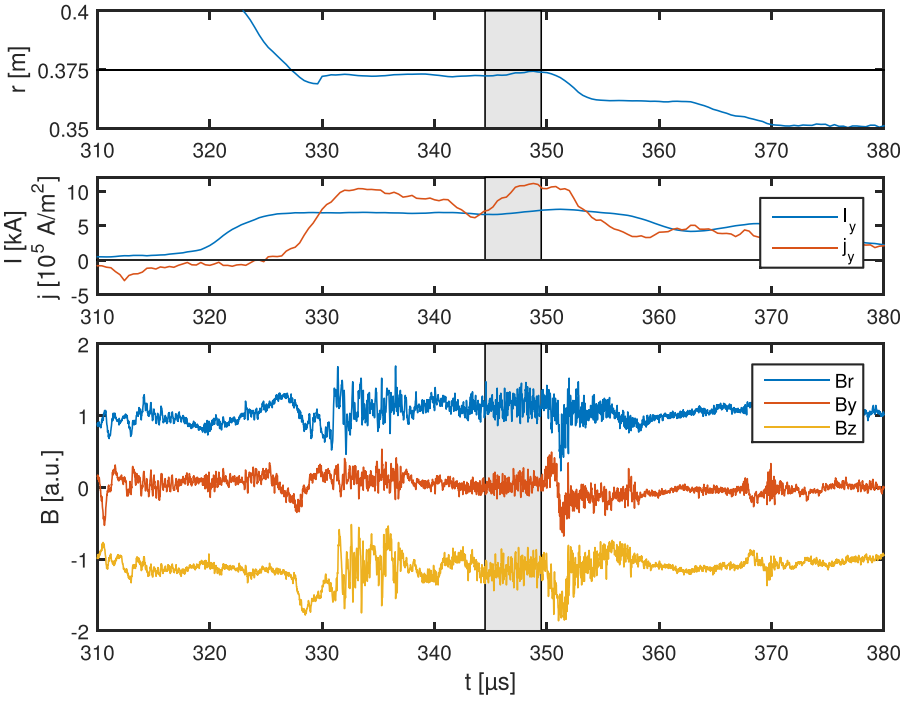

FIG. 3. Sample time traces of the radial current sheet position (top), local current density and total plasma current (center), and fluctuation probe signals (bottom) at $R = 0.375$ m for shot 169070. The gray band indicates the selected time span for further fluctuation analysis.

$n = 1-3 \times 10^{19}$ m^{-3} and electron temperatures of $T_e = 5-6$ eV. Experiments were conducted in a Helium plasma to obtain a low-collisionality regime. Guide magnetic field values, defined as the measured toroidal field amplitude at the vacuum X-point location ($R = 375$ mm and $Z = 0$), reach up to $B_g = 40$ mT and reconnecting electric fields are typically $E_\Theta = 140$–190 V/m. The top trace shows the radial trajectory of the current sheet as determined by tracking the X-point position in every time step. In this specific shot, the current sheet reaches the probe location at 330 μs and remains relatively stationary until 350 μs before moving further inwards. The total plasma current (center panel, blue) rises in response to the driven reconnection at 320 μs and remains constant around 7 kA until it begins to decay around 360 μs. The local plasma current density, evaluated from the magnetics data at the fluctuation probe location (red), is the highest during the phase in which the current sheet intersects the probe (330–350 μs). In this time span, magnetic fluctuations are observed on all three axes of the fluctuation probe (bottom panel). Though the current sheet remains largely stationary, the raw signal traces show considerable variation in amplitude and structure throughout this phase, demonstrating the high intermittency of the observed fluctuations. The shaded area is centered around the selected time point for further processing of this shot with a window of 5 μs. In this time window, the reconnection rate E_Θ (not shown) is stationary at the X-point, and density and electron temperature in the current sheet vary slowly.

A. Guide field parameter dependence

A scan of over 200 shots at varying guide field coil currents but otherwise constant discharge parameters (except for minor timing and equilibrium field adjustments to ensure current sheet reproducibility) shows how the reconnection parameters in MRX depend on the applied guide field. Figure 4 shows selected parameter dependencies: On the left, the measured X-point guide field $B_{y,X}$ (blue) and the reconnecting field B_{rec} measured 5 cm upstream of the X-point are plotted against the applied (vacuum value) guide field. Several effects are apparent here: The guide field is compressed and amplified compared to the vacuum values by up to a factor of 2 (dashed line: unity). This effect is attributed to a pileup of toroidal magnetic flux due to the way reconnection is driven in MRX, where compressive plasma flows are established toward conducting flux cores in the downstream, which does not readily allow toroidal flux to leave the system.[12] A novel observation in these experiments, which was not reported previously, is the systematic increase in the upstream field as well as with the applied guide field, even with the same reconnection drive. Compared to previous results,[32] these experiments use the upstream drive coil to maintain high physical reconnection rates E_Θ over the whole guide field range. The upstream reconnecting field increases and then saturates past 10 mT applied guide field, which is due to an identical behavior of the integrated plasma current $I_y = \int j_y dA$. While the local X-point current density and current sheet width do not exhibit a strong guide field dependence, the rise instead stems from an increased current sheet length. These two relations result in a highly nonlinear dependence of the normalized guide field value $B_{y,X}/B_{z,up}$, which rises quickly from 0 to 0.7 below 4 mT applied field and then tapers off to a maximum of around 2 at the highest values.

On the right, the normalized reconnection rate $E_{y,X}/(v_A B_{rec})$ with the reconnection rate $E_{y,X}$ at the X-line and the Alfvén velocity using the upstream reconnecting field B_{rec} and plasma density measured within the current sheet are observed to rapidly decrease with the increasing (normalized) guide field. This effect is qualitatively similar to that reported in Ref. 12. However, in the present context with the upstream drive coils, we note that the physical reconnection rate $E_{y,X}$ remains relatively constant with only moderate reduction across the guide field values. Instead, the decrease in the normalized rate with the rising guide field is mostly attributable to the increase in B_{rec}, a flux pileup effect.

B. Fluctuation profiles and spectra

Radial fluctuation profiles are obtained from the method outlined in Fig. 2. Figures 5 and 6 summarize the results of the radial fluctuation probe scans at several guide fields, referred to in the following as zero ($B_y/B_z = 0$), medium (0.6), and high (1.2).

Power spectra measured at the X-point are shown in Fig. 5 and display a broadband spectral distribution that follows a power law. The spectra (averaged over shots and pickup coil orientations) were recorded over a total of 20 shots each at the current sheet center. They are computed from the wavelet transformed data as described above, averaged per shot over a time window of 5 μs centered

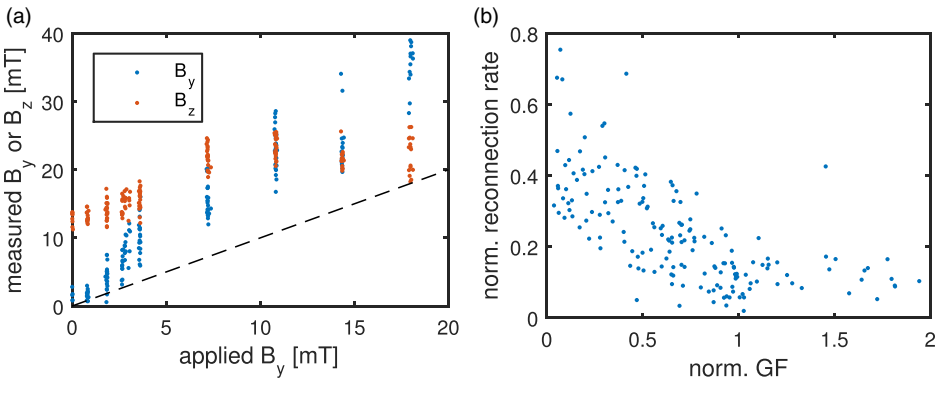

FIG. 4. Guide field parameter dependencies. Left: actual guide field amplitude (blue) and reconnecting magnetic field (red) vs. applied guide field. Right: normalized reconnection rate $E/(v_A B_{rec})$ vs. normalized guide field B_g/B_{up}.

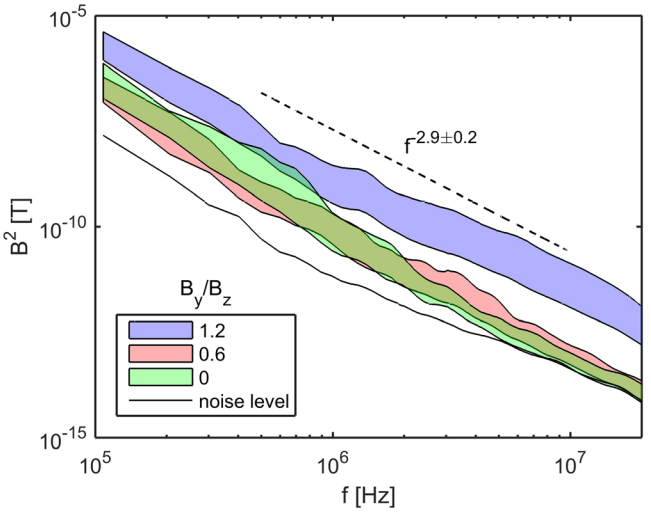

FIG. 5. Average power spectra at the current sheet center for three guide field settings, averaged over all spatial components.

around the time point of current sheet and magnetic probe intersection. The colored band delimits a standard deviation over the shot ensemble. The black line is a power spectrum of measured noise at the beginning of the shot cycle before plasma breakdown, corresponding to a realistic baseline noise level. All spectra show a clear separation from the noise floor and display a broadband, turbulent distribution over the two decades resolved by the probes. They follow a power law (with a spectral index of approximately -2.9) and are otherwise largely featureless, with no apparent characteristic frequencies such as the ion cyclotron frequency ($\approx 10^5$ Hz) and lower hybrid frequency ($\approx 5 \times 10^6$ Hz) that fall into this range. As the guide field increases, a clear rise in fluctuation power across the entire accessible frequency band is observed; however, the spectral index is largely unchanged.

The fluctuation power profiles shown in Fig. 6 show a clear correlation with the peaked current density profiles consistent with previous observations in anti-parallel reconnection,[22] together with the organization of fluctuating components to be perpendicular to the guide field. They are generated using the X-point position correction approach described in Sec. II. The frequency band chosen for power summation here is $1 < f < 10$ MHz, which gives cleaner profiles due to the absence of shot noise and low frequency changes in the current sheet structure but does not modify their overall structure. The colored bands correspond to the Monte-Carlo error estimate for each B-field component, while the black line indicates the corresponding current sheet profile. All fluctuation power profiles are strongly peaked at the X-line and are well correlated with the local current density regardless of the applied guide field. As the guide field ratio increases from 0 (left) through 0.6 (center) to 1.2 (right), three effects can be observed. First, the fluctuations become less intermittent, i.e., more consistent, with the rising guide field, as apparent in the decreasing size of the error bands with the increasing field. Second, the overall fluctuation amplitudes sharply rise in the highest guide field case (note the modified ordinate scale). Finally, the amplitude of the in-plane components, which overlap with the guide field aligned (y) component within their error bars for the zero guide field case, begins to separate and is more than two times as large as that under a high guide field. This organization, with $\tilde{\mathbf{B}}$ rotating in the poloidal plane, suggests wave propagation increasingly aligned with the guide field. Together, these indicate that the waves become both more consistent and more organized by the presence of the guide field.

Figure 7 summarizes these observations. Here, the fluctuation power at the current sheet center is integrated over the frequency range of 0.3–10 MHz and is plotted as a function of the relative guide field both as absolute power and as power normalized to the upstream magnetic field. The error bars correspond to the error bands in Fig. 6. At the highest guide field, we observe the strong increase in total power, as well as the organization of fluctuating components to be perpendicular to the guide field. However, when normalized to the upstream magnetic field, the scaled fluctuation power remains relatively unchanged within the margin of error, except for a decrease in the guide field aligned component B_y. This underscores the importance of the flux pileup effect with guide field documented in Fig. 4. This supports an intuitive picture in which the upstream, reconnecting field directly provides the energy input driving the fluctuations at the current sheet center. The fluctuations obtain a fraction $\lesssim 1\%$ of the energy input and therefore do not themselves significantly occupy a significant fraction of the converted energy, though they may mediate the conversion process to other channels such as by heating electrons.

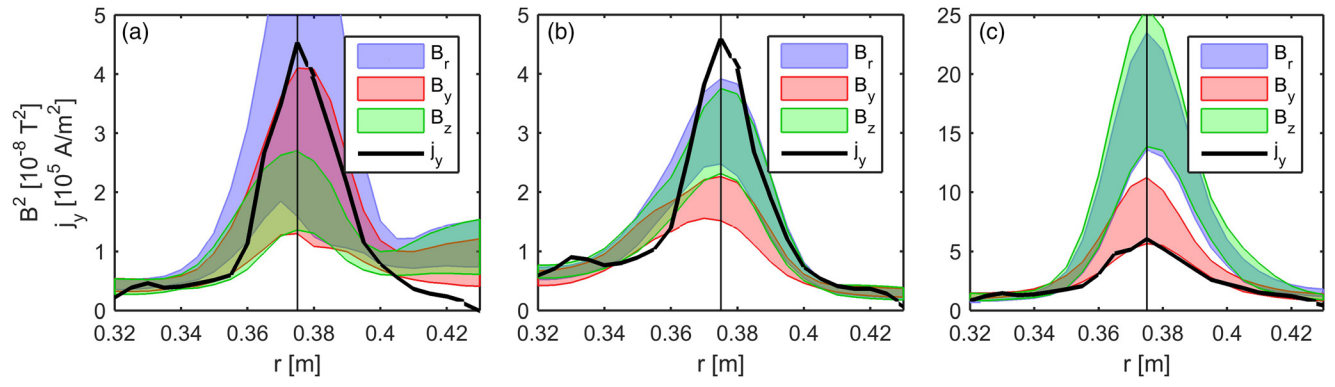

FIG. 6. Average high frequency radial fluctuation power profiles at three guide field settings with 1σ error bands (left: 0, center: 0.6, right: 1.2). Black line: current density profiles. Note the increased ordinate scale on the right.

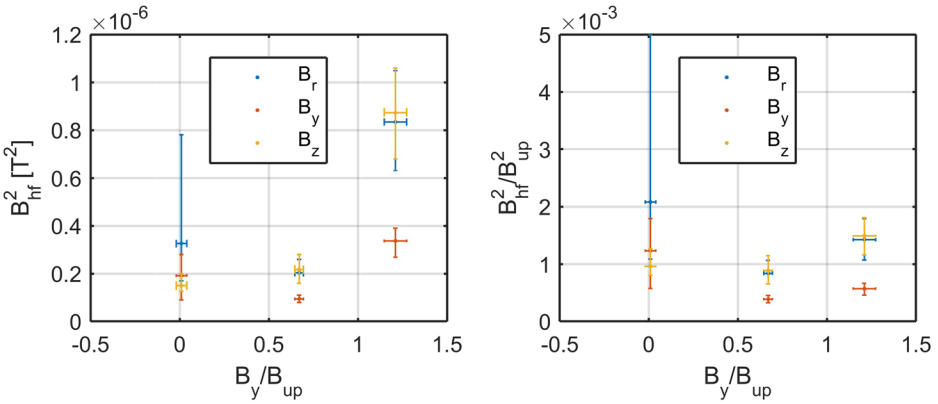

FIG. 7. Fluctuation power versus guide field, both (a) physical fluctuation power and (b) normalized to upstream magnetic energy.

C. Propagation properties

Since the results above have shown that the observed fluctuations are intermittent and turbulent, large amounts of fluctuation data were required to properly reconstruct statistically significant wave propagation properties. For this purpose, separate runs of 50 shots at each guide field setting were performed with the probe at the current sheet center, which were then processed with the wavelet hodogram method described in Sec. II. From each wavelet coefficient triplet from the three pickup coils, we compute the signed ellipticity (with regard to the equilibrium magnetic field $\mathbf{B}_0$) value $\varepsilon(f_i, t_i)$ and the normalized, instantaneous wave vector direction $\hat{k}(f_i, t_i)$. These are weighted by their cross power and then assigned to histograms $S(f, \varepsilon)$ and $S(f, \theta)$, where θ is the angle between $\hat{\mathbf{k}}$ and $\mathbf{B}_0$. While the hodogram method gives information on both the wave propagation angles and polarization with respect to the ambient magnetic field, their propagation direction and full dispersion relation require an additional phase measurement which was unavailable during the current experimental campaign. The results of this analysis are shown for the zero and high guide field cases in Fig. 8.

At zero guide field, the ellipticity is centered around 0 (note that a value of exactly 0 is statistically not possible), indicating either predominantly linear or randomly scattered polarization. Meanwhile, in the high guide field case, the waves show a clear preference for right hand polarization up to frequencies around 3 MHz. A similar picture emerges when examining the propagation angles. In the zero guide field case, a large spread in propagation angles is apparent at all frequencies (here too, a value of zero is not possible). As the guide field is increased, this spread is reduced and a majority (around 60%) of the cross spectral power is now concentrated at small propagation angles between 0° and 35°. These results indicate that at high guide field values, the wave activity at the current sheet center transitions from erratic, incoherent waves and becomes increasingly organized as right hand polarized waves propagating along the guide field.

IV. DISCUSSION AND CONCLUSIONS

In this paper, we report a controlled study of magnetic reconnection as a function of a controllable guide field. We first quantified systematic change to the reconnection parameters, including a pileup of both the guide field in the reconnection layer and the upstream, reconnecting field. The upstream pileup leads to a decrease in the normalized

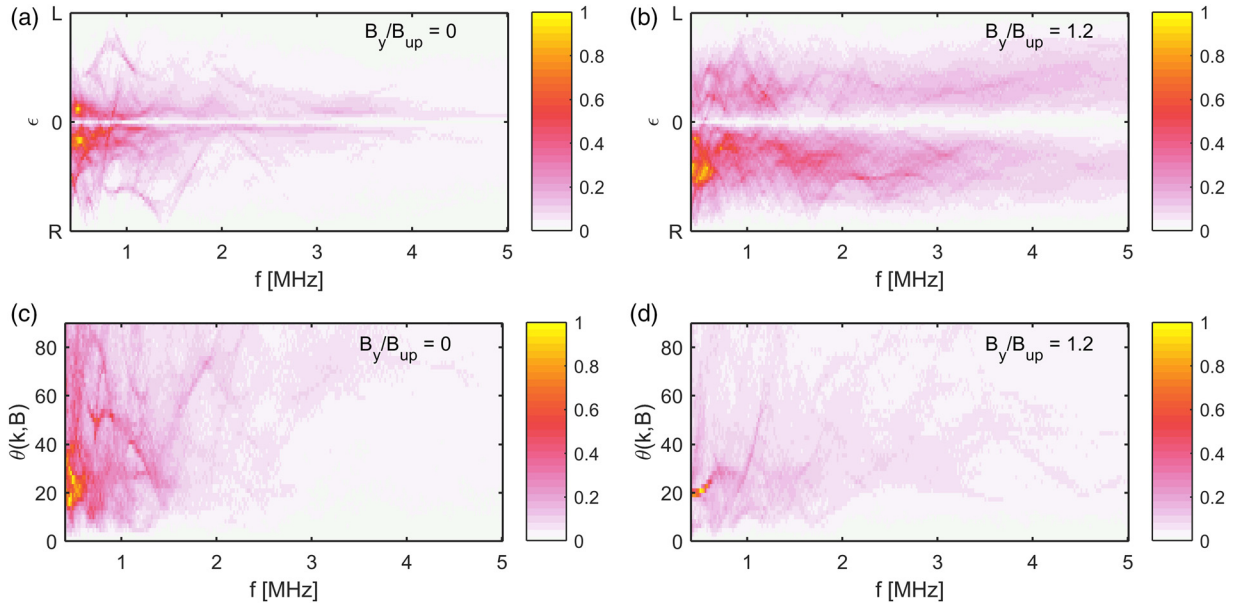

FIG. 8. Histograms of frequency-resolved signed ellipticity and angle between $\mathbf{k}$ and $\mathbf{B}_0$ for the zero (left) and high (right) guide field case.

reconnection rate $E_y/v_{A,up}B_{up}$ with the increasing guide field, even as the physical rates are comparable.

With this basis, magnetic fluctuations are studied during reconnection as a function of the guide field. Magnetic fluctuations are observed at all guide field values within the current sheet, sharply peaking at the center and correlating well with the current density profiles. The wave amplitude spectra are broadband and follow a power law, thereby possibly indicating turbulent energy dissipation. Further analysis at the current sheet center shows that at high guide fields, these fluctuations can be identified as right-hand polarized, whistler-like waves that propagate at a small angle to the mean field. As the guide field is increased, fluctuation amplitudes rise sharply, and the fluctuations become organized predominantly transverse to the guide field. We also find that at high guide field values, the presence of the fluctuations in the current sheet is more reproducible from shot-to-shot than previously observed at MRX.[22]

We now present some further discussion of the identification of the waves, the instability mechanism, and possible role providing anomalous dissipation. The results show some significant new findings which should be considered to understand the identity and driving mechanism of the waves.

The present results complement previous electromagnetic fluctuation measurements at MRX in anti-parallel reconnection,[22] which identified right-hand polarized, whistler-like waves, but only at the current sheet edge. In the present case, the guide field appears to organize the wave propagation, which allows identification of the waves within the current sheet itself. The increased organization of the spatial components and narrowing of the angular distribution of the mean **k** vector at higher guide fields are consistent with the fact that the equilibrium magnetic field is clearly defined well into the reconnection layer. By contrast, in anti-parallel reconnection, this field is by definition erratic at the X-point, so it is not surprising that the statistically inferred wave hodograms are also much more erratic.

Previous theoretical understanding of electromagnetic fluctuations in MRX showed that viable candidates included the modified two-stream instability[22] or a generalized electromagnetic lower-hybrid instability.[27] Both of these instabilities tap the free energy in the cross-field flows, including diamagnetic drifts. The cross-field character is essential to these instabilities, which overcome the fact that the parallel resonances can be a relatively weak drive mechanism unless the electron drift $v_{||} = j_{||}/ne$ is large, $v_d \gtrsim v_{te}$, i.e., for a Buneman instability.[33] This has some important implications when compared to the present observations. We recall that the wave activity remains strong in the guide field cases; indeed, the amplitude is the largest in the case with the largest guide field, and the center of the current sheet, where the waves and plasma current are most-parallel to the field, is also the location of the strongest wave activity. However, the strong guide field case is precisely when the flows are *least* cross-field, and at the center of the current sheet, the drift is completely parallel to the field. Therefore, these results contradict the basic intuition of the cross-field drift mechanisms. This should motivate further theoretical effort to find instability drive mechanisms spanning parallel and cross-field drift regimes.

A second point to address is the relationship of these waves to providing anomalous dissipation in the reconnection layer. As discussed previously, even including two-fluid effects, there remains an electron diffusion region where other terms must balance the reconnection electric field, and furthermore, in the present experiment, collisional dissipation is not sufficient in the EDR.[13] In general, quantifying the anomalous resistivity from waves is a large experimental challenge. A persistent complication is the gap between easily measurable quantities, such as fluctuation amplitudes (i.e., $\langle \tilde{B}^2 \rangle$), and those required to relate to reconnection dynamics, such as average electron momentum transfer $\langle \tilde{j}_e \times \tilde{B} \rangle$, which require non-trivial correlation measurements. Nonetheless, experimental observations provide important constraints on possible mechanisms.

Here, we first provide a simple estimate of anomalous resistivity from these waves following the assumptions made in Ref. 22. Rewriting the momentum balance including the nonlinear wave correlation yields an expression for the effective electric field

$$E_y \approx \frac{1}{ne_0}\langle \tilde{j} \times \tilde{B} \rangle \approx \frac{2}{ne_0}\left\langle k_y \frac{\gamma}{\omega}\frac{\tilde{B}^2}{\mu_0}\right\rangle. \tag{2}$$

Assuming that the fluctuations in j and B are appropriately phased for maximum resistivity and the growth rate of the instability γ is large and comparable to the wave frequency ω (a reasonable value for lower hybrid type instabilities) and using typical measured fluctuation amplitudes at high guide field values of $\tilde{B} = 1$–$2\,\mathrm{mT}$, this expression gives an upper bound estimate to the possible electric field contribution of

$$E_y = k_y(0.5 - 2)\,\mathrm{V/m}. \tag{3}$$

Meanwhile, the mismatch in the electric field between that provided by the measured Ohmic dissipation ($E_y = \eta j_y$) and the measured reconnection rate $E_y = \frac{\partial}{\partial t}A_\theta$ is 100–140 V/m, with the highest value corresponding to the lowest guide field. Consequently, if the observed fluctuations have wave numbers of $k_y = 50$–$280\,\mathrm{m}^{-1}$, they could account for the measured reconnection rate. Comparing these values to the wave numbers previously measured in the current sheet edge,[22] we find that these k_y values are possible, indicating that the observed fluctuations are a potential source of anomalous dissipation, at least in the high guide field case. We note the caveat that the highest-amplitude waves, which correspond to frequencies $f \lesssim 1$ MHz, obtained in the power spectrum presented in Fig. 5, happen to correspond to the *smallest* k-values, measured in Ref. 22; for example, using the linear dispersion observed there, $\omega/k_y \approx V_d$, we obtain $k_y \approx 10\,\mathrm{m}^{-1}$ at $f = 0.5\,\mathrm{MHz}$, which indicates insufficient anomalous resistivity. In any case, this motivates followup phase velocity and wavelength measurements, which were unfortunately not available for the present experiments, but which would improve the estimates of anomalous dissipation.

The above estimates notwithstanding the experimental results raise significant questions for attributing anomalous

resistivity to waves. A striking observation is the strong increase in the fluctuation level and improvement in reproducibility of fluctuations in the highest guide field. We showed how this can be understood from the simultaneous increase in the upstream fields at high guide fields due to the flux-pileup effect, leading to relatively constant *normalized* fluctuation energies $\langle \tilde{B}^2 \rangle / B_{up}^2$ between cases. Nevertheless, the *physical* reconnection rates are relatively constant between the cases, and there are therefore contradictions between the wave resistivities implied by the above estimates and the strong variation in fluctuation amplitude across all guide field regimes. Several interpretations of this observation are possible which should be pursued in future work. First, it is of course possible that the above theoretical formulas are too optimistic and that the waves do not provide anomalous resistivity in any regime or that different terms (such as $\langle \tilde{n}_e \tilde{E}_{||} \rangle$, not measured) are dominant. In this case, no scaling should be expected. We note that previous particle-in-cell simulations, with parameters matched to MRX, did not observe a significant anomalous resistivity or current-sheet broadening effect due to waves.[34] Second, it may be possible that the mismatch is due to limitations of the above theory, despite its intuitive appeal, and that improved theory or more detailed correlation measurements of $\langle \tilde{j}_e \times \tilde{B} \rangle$ will account for the variation. Finally, it is possible that the waves provide the resistivity only in high guide field cases, indicating a change of dissipation processes introduced by the magnetization of electrons in the reconnection layer and the modification of the wave driving mechanism from cross-field to parallel flows.

ACKNOWLEDGMENTS

This work was supported by the Max-Planck Princeton Center for Plasma Physics, funded by the U.S. Department of Energy under Contract No. DE-AC0204CH11466 and NASA under Agreements Nos. NNH15AB29I and NNH14AX631.

[1]M. Yamada, R. Kulsrud, and H. T. Ji, Rev. Mod. Phys. **82**, 603 (2010).
[2]S. Masuda, T. Kosugi, H. Hara, S. Tsuneta, and Y. Ogawara, Nature **371**, 495 (1994).
[3]M. Oieroset, T. D. Phan, M. Fujimoto, R. P. Lin, and R. P. Lepping, Nature **412**, 414 (2001).
[4]S. Günter, Q. Yu, K. Lackner, A. Bhattacharjee, and Y. M. Huang, Plasma Phys. Controlled Fusion **57**, 014017 (2015).
[5]J. B. Taylor, Rev. Mod. Phys. **58**, 741 (1986).
[6]R. J. Hastie, Astrophys. Space Sci. **256**, 177 (1997).
[7]M. Swisdak, J. F. Drake, M. A. Shay, and J. G. McIlhargey, J. Geophys. Res.: Space Phys. **110**, A05210, https://doi.org/10.1029/2004JA010748 (2005).
[8]W. Gekelman and R. L. Stenzel, J. Geophys. Res. **89**, 2715, https://doi.org/10.1029/JA089iA05p02715 (1984).
[9]J. Egedal, W. Fox, N. Katz, M. Porkolab, K. Reim, and E. Zhang, Phys. Rev. Lett. **98**, 015003 (2007).
[10]W. Fox, M. Porkolab, J. Egedal, N. Katz, and A. Le, Phys. Rev. Lett. **101**, 255003 (2008).
[11]N. Katz, J. Egedal, W. Fox, A. Le, A. Vrublevskis, and J. Bonde, Phys. Plasmas **18**, 055707 (2011).
[12]T. D. Tharp, M. Yamada, H. Ji, E. Lawrence, S. Dorfman, C. E. Myers, and J. Yoo, Phys. Rev. Lett. **109**, 165002 (2012).
[13]W. Fox, F. Sciortino, A. v. Stechow, J. Jara-Almonte, J. Yoo, H. Ji, and M. Yamada, Phys. Rev. Lett. **118**, 125002 (2017).
[14]A. von Stechow, O. Grulke, and T. Klinger, Plasma Phys. Controlled Fusion **58**, 014016 (2016).
[15]A. Y. Aydemir, Phys. Fluids B: Plasma Phys. (1989-1993) **4**, 3469 (1992).
[16]X. Wang and A. Bhattacharjee, Phys. Rev. Lett. **70**, 1627 (1993).
[17]R. G. Kleva, J. F. Drake, and F. L. Waelbroeck, Phys. Plasmas **2**, 23 (1995).
[18]X. Wang, A. Bhattacharjee, and Z. W. Ma, J. Geophys. Res.: Space Phys. **105**, 27633, https://doi.org/10.1029/1999JA000357 (2000).
[19]P. L. Pritchett and F. V. Coroniti, J. Geophys. Res. **109**, A01220 (2004).
[20]M. Hesse, Phys. Plasmas **13**, 122107 (2006).
[21]T. A. Carter, H. Ji, F. Trintchouk, M. Yamada, and R. M. Kulsrud, Phys. Rev. Lett. **88**, 015001 (2002).
[22]H. Ji, S. Terry, M. Yamada, R. Kulsrud, A. Kuritsyn, and Y. Ren, Phys. Rev. Lett. **92**, 115001 (2004).
[23]W. Fox, M. Porkolab, J. Egedal, N. Katz, and A. Le, Phys. Plasmas **17**, 072303 (2010).
[24]C. Cattell, J. Wygant, F. S. Mozer, T. Okada, K. Tsuruda, S. Kokubun, and T. Yamamoto, J. Geophys. Res. **100**, 11823, https://doi.org/10.1029/94JA03146 (1995).
[25]S. D. Bale, F. S. Mozer, and T. Phan, Geophys. Res. Lett. **29**, 33, https://doi.org/10.1029/2002GL016113 (2002).
[26]F. D. Wilder, R. E. Ergun, K. A. Goodrich, M. V. Goldman, D. L. Newman, D. M. Malaspina, A. N. Jaynes, S. J. Schwartz, K. J. Trattner, J. L. Burch, M. R. Argall, R. B. Torbert, P. A. Lindqvist, G. Marklund, O. Le Contel, L. Mirioni, Y. Khotyaintsev, R. J. Strangeway, C. T. Russell, C. J. Pollock, B. L. Giles, F. Plaschke, W. Magnes, S. Eriksson, J. E. Stawarz, A. P. Sturner, and J. C. Holmes, Geophys. Res. Lett. **43**, 5909, https://doi.org/10.1002/2016GL069473 (2016).
[27]H. T. Ji, R. Kulsrud, W. Fox, and M. Yamada, J. Geophys. Res. **110**, A08212, https://doi.org/10.1029/2005JA011188 (2005).
[28]W. Fox, M. Porkolab, J. Egedal, N. Katz, and A. Le, Phys. Plasmas **19**, 032118 (2012).
[29]M. Yamada, J. Yoo, J. Jara-Almonte, H. Ji, R. Kulsrud, and C. Myers, Nat. Commun. **5**, 4774 (2014).
[30]J. Jara-Almonte, Ph.D. thesis, Princeton University (2017).
[31]B. P. van Milligen, C. Hidalgo, E. Sanchez, M. A. Pedrosa, R. Balbin, I. GarciaCortes, and G. R. Tynan, Rev. Sci. Instrum. **68**, 967 (1997).
[32]T. D. Tharp, M. Yamada, H. Ji, E. Lawrence, S. Dorfman, C. Myers, J. Yoo, Y. M. Huang, and A. Bhattacharjee, Phys. Plasmas **20**, 055705 (2013).
[33]N. A. Krall and P. C. Liewer, Phys. Rev. A **4**, 2094 (1971).
[34]V. Roytershteyn, S. Dorfman, W. Daughton, H. Ji, M. Yamada, and H. Karimabadi, Phys. Plasmas **20**, 061212 (2013).